PROCEEDINGS OF SCIENCE

ONLINE ICRC 2021
THE ASTROPARTICLE PHYSICS CONFERENCE
Berlin | Germany
37th International Cosmic Ray Conference
12–23 July 2021

New Constraints on Cosmic Particle Populations at the Galactic Center using X-ray Observations of the Molecular Cloud Sagittarius B2

Field Rogers,[a,*] **Shuo Zhang,**[b] **Kerstin Perez,**[a] **Maïca Clavel**[c] **and Afura Taylor**[a]

[a] *Massachusetts Institute of Technology,*
77 Massachusetts Ave, Cambridge, MA 02139 USA
[b] *Bard College,*
30 Campus Road, Annandale-on-Hudson, NY 12504 USA
[c] *Univ. Grenoble Alpes,*
CNRS, IPAG, 38000 Grenoble, France
E-mail: frrogers@mit.edu

Located ∼100 pc from the dynamic center of the Milky Way, the molecular cloud Sagittarius B2 (Sgr B2) is the most massive such object in the Galactic Center region. In X-rays, Sgr B2 shows a prominent neutral Fe Kα line at 6.4 keV and continuum emission beyond 10 keV, indicating high-energy, non-thermal processes in the cloud. The Sgr B2 complex is an X-ray reflection nebula whose total emissions have decreased since the year 2001 as it reprocesses what are likely one or more past energetic outbursts from the supermassive black hole Sagittarius A*. The X-ray reflection model explains the observed time-variability of the Fe Kα and hard X-ray emissions, and it provides a window into the luminous history of our nearest supermassive black hole. In light of evidence of elevated cosmic particle populations in the Galactic Center, recent interest has also focused on X-rays from Sgr B2 as a probe of low-energy (sub-GeV) cosmic particles. In contrast to X-ray reflection, in this case we can assume that the X-ray flux contribution from ionization by low-energy cosmic particles is constant in time, such that upper limits on low-energy cosmic particle populations may be obtained using the lowest flux levels observed from the cloud. Here, we present the most recent and correspondingly dimmest *NuSTAR* and *XMM-Newton* observations of Sgr B2, from 2018. These reveal small-scale variations within lower density portions of the Sgr B2 complex, including brightening features, and enable the best upper limits on ionization of molecular clouds by low-energy cosmic particles in the inner ∼ 100 pc of the Galaxy.

37th Internationral Cosmic Ray Conference (ICRC 2021)
July 12th – 23rd, 2021
Online – Berlin, Germany

*Presenter

PoS(ICRC2021)288

1. Introduction

Centered ∼100 pc from the supermassive black hole Sagittarius A* (Sgr A*) at the center of the Galaxy, and ∼8 kpc from Earth, the molecular cloud (MC) Sagittarius B2 (Sgr B2) is the densest and most massive cloud in the Central Molecular Zone (CMZ), a region that extends several 100 pc from Sgr A* and contains ∼10% of the Galaxy's molecular material [1]. X-ray observations of Sgr B2 have revealed a strong neutral Fe Kα line at 6.4 keV [2–8] as well as a hard continuum up to 60 keV [5, 9, 10]. These features imply energetic, non-thermal interactions capable of ionizing the K-shell electrons of neutral Fe and have made Sgr B2 an object of interest for decades. The X-ray picture is further complicated by the time-varying nature of the emission. Since the peak flux was last observed in 2001, the Fe Kα emission has decreased monotonically, down to ∼ 20% of the peak by 2013 [8, 10], and the continuum emission has decreased commensurately [5].

In a simplified model, Sgr B2 consists of a dense ($(3-9)\times10^6$ H$_2$ cm^{-3}) star-forming core with radius $\sim 2-4''$ ($\sim 0.15-0.3$ pc given ∼8 kpc distance to Sgr B2). The core is surrounded by an envelope of intermediate density (10^4-10^5 H$_2$ cm^{-3}) with radius ∼2.2′, and a diffuse ($\sim10^3$ H$_2$ cm^{-3}) region with radius ∼9.9′ for a total column density N_H $\sim10^{24}$ cm^{-2} through the core and mass $\sim 6\times10^6 M_\odot$ [11, 12] . The true structure is more complicated, including several subdominant cores [13–15] and a non-uniform shape as revealed by images of cold dust [16] .

In the X-ray reflection nebula (XRN) model, the Fe Kα X-rays originate in the reprocessing of external X-rays via K-shell photoionization of neutral Fe while the continuum emission arises from inverse Compton scattering [2, 17]. Reprocessing of X-rays from past flaring activity of Sgr A* is the widely accepted origin of the time-variable Sgr B2 X-ray emission. An outburst with luminosity $L_x \sim 10^{39}$ erg s^{-1} several hundred years ago lasting $\gtrsim$10 years [2, 5], or a shorter, brighter event taking >10 years to traverse the cloud [8], could produce the observed light curve. Though direct observation reveals that Sgr A* is presently in a quiescent state [18], the XRN model of the CMZ clouds overall reveals that Sgr A* has been brighter in the past few hundred years with at least two short outbursts [8, 19]. Meanwhile, indication of the brilliance of Sgr A* in the more distant past, $>10^6$ years ago, comes from the Fermi Bubbles, likely formed in an AGN phase of Sgr A* [20].

A portion of the Sgr B2 X-ray emission could instead arise from low-energy (<1 GeV, i.e. highly ionizing) cosmic-ray (LECR) electrons or protons, where the Fe Kα line arises from K-shell ionization of neutral Fe and the continuum arises from Bremsstrahlung processes [21, 22]. Neither electrons nor protons can explain the full time-varying flux, as the cooling time for ∼100 MeV protons is too long [5], while LECR electrons require a highly tuned model to explain the peak flux [23]. However, any LECRs in the cloud would contribute to the total X-ray flux.

Evidence for elevated LECR populations in the Galactic Center (GC) region relative to the local Galactic environment comes from modeling observed hydrogen ionization rates. Populations of LECR protons, electrons, or both could explain excess ionization in the CMZ [24]. Additionally, CRs in a broad energy range have been invoked to explain non-thermal emissions from the GC at a range of wavelengths. TeV-scale γ-ray emission from the GC molecular clouds and centered on Sgr A* have been taken as evidence of protons up to a few PeV [25]. Meanwhile, nonthermal radio filaments have been interpreted as synchrotron radiation from GeV-scale electrons [23].

The origin of GC CRs is an open topic of discussion. While acceleration up to ∼100 TeV is typically credited to Supernova remnants (SNR), it is unclear if SNR can be responsible for the GC

CRs present today. Further, PeV-scale cosmic protons cannot be accelerated in most SNR models and may be attributable to past activity of Sgr A* [25]. Other discussions consider the Fermi bubbles [26], and star-forming clusters [27] as possible PeVatrons, and possible GC accelerators include pulsars, stellar winds, and magnetic reconnection. Molecular cloud-based constraints on GC LECRs will contribute to the overall GC cosmic ray picture.

Measuring X-ray fluxes enables setting upper limits on LECRs within a given region of Sgr B2, as has been the focus of several previous studies [5, 10, 22, 24, 28]. The absolute CR populations have been inaccessible due to uncertainty in the time-variable XRN component, but previous discussion has assumed Sgr B2 would soon reach a constant flux such that the internal CR population could be extracted. The ability of CRs to traverse MCs, and thus extrapolation to limits on ambient external GC CR populations, is highly model dependent and is discussed in Section 5.

In this contribution, we use joint observations of Sgr B2 obtained in 2018 by the *XMM-Newton* and *NuSTAR* X-ray telescopes, and we also make use of archived *XMM-Newton* observations from 2001, 2004, and 2012. In Section 2 we show the X-ray morphology of Sgr B2 while in Section 3 we present X-ray spectra from central region. In Section 4 we compare the 2018 flux to earlier data to discuss the continued decrease in X-ray reflection since 2001, and in Section 5, we set upper limits on ambient LECR proton and electron populations in different regions of Sgr B2 and in the context of the surrounding CMZ.

2. Morphology of X-ray Emission

Figure 1 shows the morphology of the Sgr B2 cloud as observed in 2018 by *XMM-Newton* and *NuSTAR*. The *XMM-Newton* Fe Kα line map shows that the core of Sgr B2 is detected at 13σ significance within the envelope region. The core is also detected by *NuSTAR* from 10 – 20 keV. Above 20 keV, the *NuSTAR* observation is dominated by background, and the core is not significantly detected ($< 3\sigma$).

In addition to the central core and envelope, Fe Kα emission is detected at $> 5\sigma$ significance from four substructures within the diffuse region of Sgr B2 in the projected plane. Two of these substructures coincide spatially with the cloud features previously identified as G0.66-0.13 and G0.56-0.11 [8, 10]. The other two substructures have no previously reported counterpart and are identified here as G0.61+0.00 and G0.75-0.01. G0.66-0.13 and G0.61+0.00 lie within the *NuSTAR* field of view but are not resolved above background in the higher energy bands.

3. Spectral Analysis

Figure 2 (left) shows the spectra extracted from the central region of Sgr B2 as observed in 2018, overlaid with the best fits to a phenomenological model obtained using `XSPEC` spectral fitting software. We used the phenomenological model to directly fit the fluorescent line (gaussian) and continuum (powerlaw) spectral components, and we evaluated the fit on the basis of χ^2_ν. We additionally fitted the data with the `LECRe` and `LECRp` spectral models from [22], which are based on a simulation of LECRs in MCs, and with three X-ray reprocessing spectral models [30–32]. All fits additionally included a thermal plasma component (`apec`) and accounted for internal and foreground absorption using the `XSPEC` model `wabs`. Throughout this work, we used the phenomenological

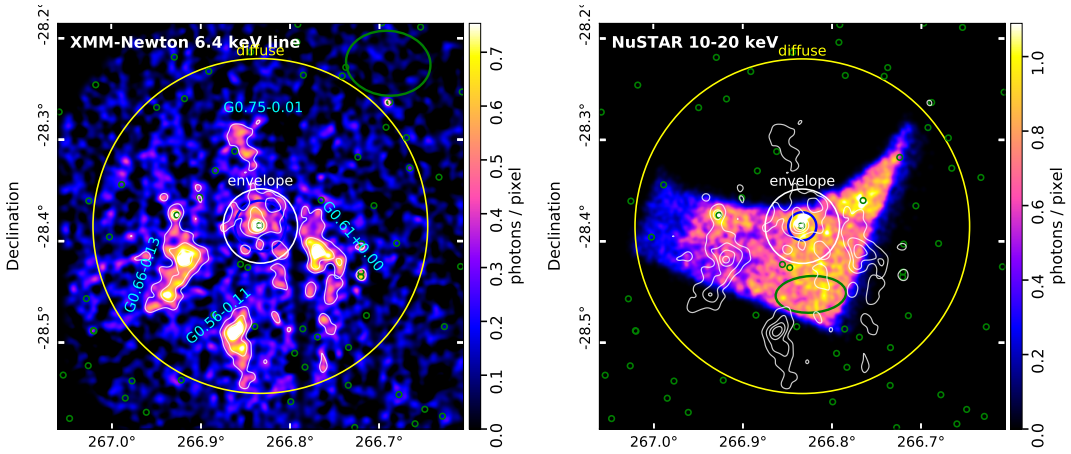

Figure 1: The 2018 X-ray morphology of the $24' \times 24'$ region surrounding Sgr B2 is shown as observed by *XMM-Newton pn* instrument in the 6.4 keV line (left) by *NuSTAR FPMA* instrument in the $10 - 20$ keV energy band (right). The 6.4 keV line image was prepared by subtracting a continuum band, $5.8 - 6.2$ keV, from a $6.2 - 6.6$ keV signal band. Contours (white) of the *XMM-Newton* 6.4 keV map are overlaid on both images and illuminate several substructures, labelled by their Galactic coordinates (cyan text), in addition to the core and envelope of Sgr B2. In *NuSTAR FPMA*, contamination by photons not processed by instrument optics ("stray light") from a bright off-axis source is evident the radial region removed from the top-left of the image. Meanwhile stray light from diffuse sources is present throughout the *NuSTAR* field of view. Circles indicating the boundaries of the diffuse (yellow, $9.9'$ radius) and envelope (white, $2.2'$ radius) regions of the simplified model are overlaid, while the core ($2 - 4''$ radius) is smaller than the angular resolution of both telescopes. The brightest ($> 2 \times 10^{-6}$ ph s^{-1} in $2 - 8$ keV) hard X-ray sources from the Chandra catalog [29] are shown (green circles), as well as the $90''$ (*XMM-Newton*) and $50''$ (*NuSTAR*– reduced due to stray light contamination) regions from which spectra were extracted (blue) and the respective elliptical regions used for background subtraction while extracting spectra (green). Color bars indicate intensity in photons per pixel.

model to evaluate the Fe Kα line intensity from different regions of Sgr B2. Details of the spectral extraction, models, and fitting are in a publication in preparation [33].

4. Time Variability of the X-ray Flux

Figure 2 (right) shows the change in flux from the central $90''$ of Sgr B2 over time, with the 2018 observations showing a ~50% decrease in emissions from the central $90''$ relative to 2012. This indicating that the 2012 flux from the core and envelope was dominated the time-varying X-ray reprocessing component. To probe if the 2018 emissions represented the constant background flux or were still dominated by the time-variable X-ray reprocessing component, the light curve from the central $90''$ was fitted to an exponential decrease with a constant offset. However, the fit was under-constrained, and the data were consistent with both a constant offset of 0 and a constant offset of the 2018 flux level. Based on the indeterminate light curves, and the satisfactory fitting with all spectral models in Section 3, the data are agnostic on the question of whether the 2018 emissions arise primarily from X-ray reprocessing versus LECR ionization. Accordingly, we only set upper limits on LECR populations in this work.

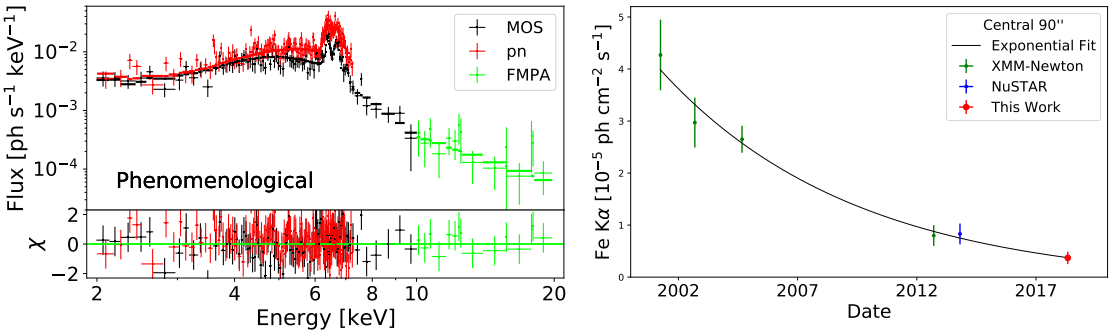

Figure 2: *Left:* The 2018 spectra of the central 90″ of Sgr B2 as observed by the *XMM-Newton MOS* (black, 2 – 10 keV) and *pn* (red, 2 – 7.8 keV) instruments and the inner 50″ by *NuSTAR FPMA* (green, 10 – 20 keV) are fitted with the phenomenological model to extract the Fe Kα line flux. The *XMM-Newton* (*NuSTAR* data are binned with 3σ (1.5σ) errors. The best fit, which had $\chi^2_\nu = 0.97$ for 256 degrees of freedom, is shown in the horizontal lines. *Right:* The Fe Kα light curve from from the central 90″ is shown, with past *XMM-Newton* (green) and *NuSTAR* (blue) data points from [10] and the 2018 flux as calculated in this work. The light curve was fitted to an exponential decrease with a constant offset. However, the best fit constant offset was compatible with both the 2018 flux level and 0 flux. The light curve could not constrain whether the flux had reached a constant value by 2018 or if it was still decreasing.

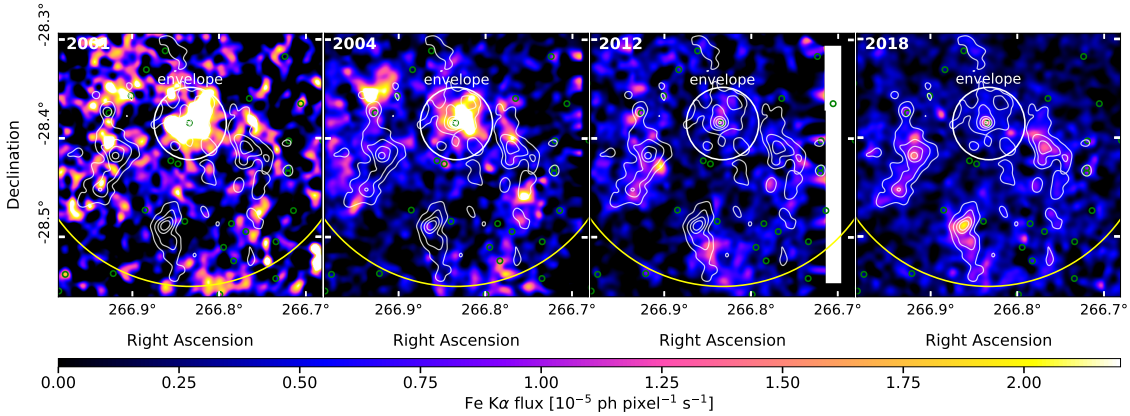

Figure 3: The overall decrease in Fe Kα emission since 2001 from core, envelope, and diffuse region of Sgr B2 is illustrated in continuum-subtracted and exposure-corrected *XMM-Newton (pn)* observations from 2001 (first panel), 2004 (second panel), 2012 (third panel) and 2018 (fourth panel). The images are overlaid with contours of the 2018 observation from Figure 1. The data also show substructures within the diffuse region which brighten and dim over time.

Figure 3 illustrates the time-varying morphology Fe Kα emissions from the Sgr B2 complex using continuum-subtracted and exposure-corrected images. Consistent with the spectral fitting results, the Fe Kα flux from the Sgr B2 core and envelope, as well as the total flux from the complex over all, has decreased over time. In contrast, the images show that the substructures such as those identified in Figure 1 do not decrease steadily over time. Instead, different substructures from within the diffuse region brighten and dim in each observation. This behavior complicates the picture of Sgr B2 emissions dimming to a constant flux dominated by LECR interactions as

the XRN component fades. Instead, efforts to probe LECR interactions in the cloud continue to contend with brightening and dimming substructures.

5. Ambient Low-energy Cosmic Rays

In 2018, the Fe Kα flux from the core and envelope of Sgr B2 was the lowest yet observed. Since this indicates that the time-variable XRN flux was at its lowest level yet, any LECR contribution was a larger portion of the 2018 flux compared to previous observations. Therefore, using the 2018 observations, we were able to set the most accurate upper limits on LECR populations within Sgr B2 using spectral analysis.

In this section, we aim to understand the best limits in the context of ambient GC LECRs. The reduced hydrogen ionization rate within Sgr B2 compared to its surroundings provides evidence that LECRs do not freely traverse dense MCs [24]. The details of CR interactions in dense clouds are model dependent and have been the subject of several theoretical works, where the predicted geometry of energy deposition by LECRs depends on simplified models of the gas distribution and assumptions about magnetic field structure in either a general cloud or Sgr B2 specifically. Following [24], who use the simplified gas distribution, CR transport within the Sgr B2 envelope is best described as diffusion on by turbulent magnetic fluctuations, which arise from interactions of turbulent neutral gas with ionized hydrogen. Meanwhile, diffusion is negligible in the diffuse cloud region, where turbulent magnetic fluctuations are small, such that cosmic ray propagation is determined primarily by ionization and excitation. Thus, in the simplified model, protons (electrons) with $KE \gtrsim 20\,\mathrm{MeV}$ (1 MeV) traverse the diffuse region to reach the envelope, where they propagate diffusively before being absorbed within $0.1 - 0.3\,\mathrm{pc}$ [24]. Lower-energy particles are absorbed within the diffuse region.

Given a powerlaw spectrum of LECR protons outside the cloud, the steady-state spectrum for protons reaching the envelope was calculated [24] using the relative ionization rates in and out of the cloud to find a steady-state solution. The resulting intensity of Fe Kα emission from Sgr B2 complex was $I_{6.4} \approx (3-5)\frac{Z}{Z_\odot} \times 10^{-6}\,\mathrm{ph\,cm^{-2}\,s^{-1}}$, where the range of $3-5$ depends on the powerlaw index of the ambient CR spectrum and the radius and column density of the cloud. For comparison, we extracted flux from the envelope ($0.5' - 2.2'$, excluding the core) region from the 2018 data and found $F_{6.4} = 12.7 \pm 1.2 \times 10^{-6}\,\mathrm{ph\,cm^{-2}\,s^{-1}}$. Considering the reasonable case of $Z/Z_\odot = 2$, this measurement is comparable to but still larger than calculated flux expected from the LECR proton population that provide the ionization rates in and out of Sgr B2. This means that the 2018 emission could be dominated by LECR proton interactions; should future observations show a decrease to $\lesssim 50\%$ of the 2018 Fe Kα flux, the parameter space for LECR protons in the model in [24] would be constrained.

In the LECR electron case, electrons that reach the envelope are highly relativistic, with ionization rates nearly independent of energy. Following [24], an electron density $n_e \sim 7.7 \times 10^{-8}\,\mathrm{cm^{-3}}$ is required to explain the observed hydrogen ionization in the Sgr B2 envelope. The expected X-ray continuum spectrum expected from Bremsstrahlung processes by electrons is harder than that of an LECRp- or X-ray reflection-induced continuum, with a spectral index of ~ 1. Given the population of electrons required to explain the ionization in Sgr B2, an excess in the continuum

from 20 – 60 keV should be observable given the flux levels in 2015 [24]. However, this was not observed [10], and thus, [24] do not treat fluorescence line emission from LECR electrons.

6. Conclusion

Sgr B2 is the most massive molecular cloud in the Central Molecular Zone, and its X-ray features, including a prominent Fe Kα line at 6.4 keV and a hard X-ray continuum above 10 keV, have been the subject of discussion and observation for decades. These features provide a window into past energetic activity of Sgr A*, via X-ray reprocessing in the cloud, and to any sub-GeV cosmic ray populations, via ionization and excitation.

We presented the $>$ 100 ks observations of Sgr B2 taken jointly in 2018 by the *XMM-Newton* and *NuSTAR* X-ray telescopes. These data show that the Fe Kα and hard continuum emissions from the central region of the cloud have decreased by $\sim$ 50% since the previous *XMM-Newton* (2012) and *NuSTAR* (2013) observations, indicating that the X-ray flux in all prior observations of Sgr B2 is dominated by X-ray reflection. The 2018 data are consistent with arising either primarily from X-ray reflection or primarily from cosmic ray interactions, so we have used the flux levels to set best upper limits on sub-GeV proton and electron populations within Sgr B2.

Acknowledgments

This research made use of data obtained with *XMM-Newton*, an ESA science mission with instruments and contribution directly funded by ESA Member States and NASA. This work is supported by XMM-Newton AO Cycle-16 observation grant 80NSSC18K0623. This work also made use of data from *NuSTAR*, a project led by the California Institute of Technology, managed by the Jet Propulsion Laboratory, and funded by NASA. This research has made use of data obtained through the High Energy Astrophysics Science Archive Research Center Online Service, provided by the NASA/Goddard Space Flight Center. F. Rogers is supported through the National Science Foundation Graduate Research Fellowship Program under Grant No. 1122374. M. Clavel acknowledges financial support from the French National Research Agency in the framework of the "Investissements d'avenir" program (ANR-15-IDEX-02) and from CNES.

References

[1] M. Morris & E. Serabyn, ARA&A **34** (1996) 645.

[2] K. Koyama et al., PASJ **48** (1996) 249.

[3] H. Murakami et al., ApJ **558** (2001) 687 [astro-ph/0105273].

[4] K. Koyama et al., PASJ **59** (2007) 221 [astro-ph/0609310].

[5] R. Terrier et al., ApJ **719** (2010) 143 [1005.4807].

[6] T. Inui et al., PASJ **61 S241** (2009) S241 [0803.1528].

[7] M. Nobukawa et al., ApJL **739** (2011) L52 [1109.1950].

[8] R. Terrier et al., A&A **612** (2018) A102 [1712.04232].

[9] M. G. Revnivtsev et al., A&A **425** (2004) L49

[10] S. Zhang et al. ApJ **815** (2015) 132 [1507.08740]

[11] D. C. Lis & P. F. Goldsmith, ApJ **356** (1990) 195.

[12] P. de Vicente et al., A&A 320 (1997) 957.

[13] J. M. Benson & K. J. Johnson, ApJ **277** (1984) 199.

[14] F. Sato ApJ **535** (2000) 857.

[15] M. Etxaluze, A&A **556** A137 [1307.0335].

[16] S. Molinari et al. ApJL **735** (2011) L33 [1105.5486].

[17] R. Sunyaev & E. Churazov, MNRAS **297** (1998) 1279 [astro-ph/9805038].

[18] F. Baganoff et al., ApJ **591** (2003) 891 [astro-ph/0102151].

[19] M. Clavel et al., A&A **558** (2013) A32 [1307.3954]

[20] H. Y. Yang et al., Galaxies **6** (2018) 29 [0802.03890].

[21] F. Yusef-Zadeh et al., ApJ **656** (2007) 847 [astro-ph/0608710].

[22] V. Tatischeff et al., A&A **546** (2012) A88.

[23] F. Yusef-Zadeh et al., ApJ **762** (2013) 33 [1206.6882].

[24] V. A. Dogiel et al., ApJ **809** (2015) 48 [1507.02440].

[25] HESS Collaboration, Nature **531** (2016) 476 [1603.07730].

[26] K. S. Cheng, ApJ **746** (2012) 116 [1111.512].

[27] A. Albert et al., ApJL **907** (2021) 907 [2012.15275].

[28] A. Valinia et al., ApJ **543** (2000) 733 [astro-ph/0006202].

[29] M. P. Muno et al., ApJS **181** (2009) 110 [0809.1105].

[30] T. Yaqoob, MNRAS **423** (2012) 3360 [1204.4196].

[31] M. Walls et al., MNRAS **463** (2016) 4893 [1609.00175].

[32] E. Churazov et al., MNRAS **468** (2017) 165 [1612.00180].

[33] F. Rogers et al., 2021 *in prep*.

PoS(ICRC2021)288